Journal of Power Sources 195 (2010) 435–444

Contents lists available at ScienceDirect

Journal of Power Sources

journal homepage: www.elsevier.com/locate/jpowsour

Influence of humidification on deterioration of gas diffusivity in catalyst layer on polymer electrolyte fuel cell

Y. Hiramitsu[a,*], H. Sato[a], H. Hosomi[b], Y. Aoki[b], T. Harada[b], Y. Sakiyama[b], Y. Nakagawa[b], K. Kobayashi[a], M. Hori[a]

[a] Fuel Cell Research Center, Daido University, 10-3 Takiharu-cho, Minami-ku, Nagoya 457-8530, Japan
[b] Toray Research Center Inc., 3-3-7 Sonoyama, Otsu, Shiga 520-8567, Japan

ARTICLE INFO

Article history:
Received 6 March 2009
Received in revised form 16 July 2009
Accepted 18 July 2009
Available online 28 July 2009

Keywords:
PEFC
Catalyst layer
Gas diffusion layer
Gas diffusivity
Carbon corrosion
Porosity

ABSTRACT

The effect of water on polymer electrolyte fuel cell degradation was examined with humidity as a parameter. Polymer electrolyte fuel cells were subjected to long-term operation of 10 000 h to examine the relation between decline in cell voltage and degradation of the catalyst layers or gas diffusion layers. The diffusion overpotential increased during long-term operation at relatively high humidification of 81% RH, but only in the catalyst layer and not in the gas diffusion layer. At low humidification of 52% RH, the increase in diffusion overpotential was small, indicating that the increase was more likely to occur under high humidification. Post-analysis of the catalyst layer revealed that the membrane electrode assembly had increased diffusion overpotential during operation under high humidification, as a result of the sharp decline in porosity. The increase of diffusion overpotential in the catalyst layer was also investigated by the observation of the degradation due to the oxidation of the Pt–carbon supports. However, it was found that the oxidation of carbon support which had increased diffusion overpotential was small.

1. Introduction

Polymer electrolyte fuel cells (PEFCs) generate electricity within the comparatively low temperature range from room temperature to 120 °C and have high-power density. Theoretically, these features confer advantages of faster startup and ease of miniaturization. Therefore, PEFCs are recommended for home cogeneration systems and vehicles. Research and development efforts toward the practical use of fuel cells are in progress to achieve higher power levels over longer cell lifetimes [1,2]. High-power output from the low current density region to the high current density region is particularly important for automotive applications, due to the reduction in system size. Research in automotive PEFCs has emphasized the use of pure hydrogen as a fuel and air as the oxidant, under atmospheric pressures. After entering the cell, the hydrogen and oxygen pass through the gas diffusion layer (GDL), diffuse throughout the catalyst layer (CL) and react on the Pt catalyst. The nature of the cathode has significant influence on the above process for two reasons: Firstly, the rate of reduction is much slower for oxygen than for hydrogen. Secondly, the oxygen concentration in air which is used as the oxidant is only 20%, whereas the hydrogen concentration at the cathode is 100%. Optimization of the CL structure is essential to raise the power density of the PEFC. The CL is a gas diffusion electrode with a structure that includes smaller pores than those in the GDL by a factor of 10^{-3}. Oxygen diffuses through the pores of CL and it is reduced on the catalyst. The ionomer conducts protons and the carbon support that holds the catalyst conducts the electron. Thus, the PEFC generates electricity with such a structure. Therefore, the reaction sites are limited to the triple phase boundary (catalyst, ionomer and reactant gas) [3]. In addition, the pores in the cathode catalyst allow the exit of water produced by the reaction [4].

Researchers have succeeded in raising the power density of PEFCs by expanding the catalyst surface area and improving dispersion, which has improved the utilization rates of the catalyst, ionomer and pores that constitute the triple phase boundary. (1) The specific surface area of the catalyst has been expanded by using finer catalyst particles. (2) The ionomer has been mixed to a Pt/carbon with high dispersion to expand effective catalyst surface area and to improve the distribution of pores for better gas diffusivity. (3) The utilization rates of the catalyst and ionomer have been increased by optimizing microstructure consisted of carbon particles [5–7]. Such approaches to the fabrication of the CL have improved PEFC polarization characteristics and dramatically increased power density.

* Corresponding author. Tel.: +81 52 612 6144; fax: +81 52 612 6144.
E-mail addresses: hiramitu@daido-it.ac.jp (Y. Hiramitsu), h-sato@daido-it.ac.jp (H. Sato), Hiroyuki_Hosomi@trc.toray.co.jp (H. Hosomi), Yasuhito_Aoki@trc.toray.co.jp (Y. Aoki), Takahiro_Harada@trc.toray.co.jp (T. Harada), Yoko_Sakiyama@trc.toray.co.jp (Y. Sakiyama), Yoshitsugu_Nakagawa@trc.toray.co.jp (Y. Nakagawa), k3kenji@daido-it.ac.jp (K. Kobayashi), hori@daido-it.ac.jp (M. Hori).

0378-7753/$ – see front matter © 2009 Elsevier B.V. All rights reserved.
doi:10.1016/j.jpowsour.2009.07.035

Water management during fuel cell operation is also essential to maintaining stability and good performance in a PEFC. The proton exchange membrane (PEM) used in the PEFC and the ionomer in the CL exhibits high proton conductivity under the condition of high water content. Therefore, in order to obtain higher cell performance, it is necessary to balance between humidity of supplied gases and product water. This is also accomplished by maintaining the water produced in the CL by power generation within the cell [8,9] using a microporous layer, which is placed between the CL and the GDL.

However, in the high current density region, lots of water generated is not always completely drained from the CL via the GDL. When the fuel cell is operated at a high gas utilization rate in an attempt to obtain higher efficiency, the water tends to accumulate in the CL and GDL. This is commonly referred to as flooding. The flooding causes to decrease the gas diffusivity at cathode and cell performance [10–14].

In an attempt to obtain higher performance or higher system efficiency from a PEFC, the gas blockages are occurred by flooding, which swings the cell performance. Therefore, improved water management is an essential step to obtain further advances in fuel cell performance and system efficiency.

Besides optimization of the CL structure, conventional technique for the prevention of flooding is to treat the GDL with a waterproof resin, such as polytetrafluoroethylene (PTFE). A highly waterproof GDL resists wetting, which prevents flooding by blockage of pores by water. This significantly improves the initial performance of the cell. Many reports have described how flooding in the initial stage of operation is affected by the characteristics of the GDL and the magnitude of waterproof treatment [15–21]. Several researchers have reported that the hydrophobicity of a waterproofed GDL gradually declines over time, and the gas diffusivity is also decreased [22–25]. Another problem associated with flooding over time is corrosion of the carbon support in the CL, which also deteriorates the gas diffusivity [2,26–31].

Thus, industry has aimed to increase the durability of PEFCs by developing CL and GDL materials that are less prone to degradation of the gas diffusivity over time. Such improvements will require knowledge of when, in what component(s), and how the gas diffusivity deteriorate in fuel cells over time, and how water management is involved in the deterioration of gas diffusivity. However, there are still many unsolved issues, and no guidelines have been established for the fabrication of fuel cells with the desired high durability [32].

This study addressed humidification of the gas supply during operation and examined time-related changes in cell performance, particularly time-related changes in the gas diffusivity. Long-term power generation tests were carried out for 10 000 h under conditions of high and low humidification with constant load. The fuel cells were stopped at regular intervals for examination, and factors related to the decrease in output voltage were analyzed. These cells were compared with unused cells and an attempt was made to identify the components responsible for the decline in cell voltage. Furthermore, at the end of the long-term tests, post-analyses were conducted to elucidate the influence of degradation of each material.

2. Experimental

2.1. Long-term operation test

2.1.1. GDL and waterproof treatment

TGP-H-H090 (Toray Industries, Inc., Japan) was used as GDL, which thickness was 280 μm in low humidification test. A thinner prototype GDL manufactured by Mitsubishi Rayon Co., Ltd., Japan, which thickness of 100 μm was used in high humidification test.

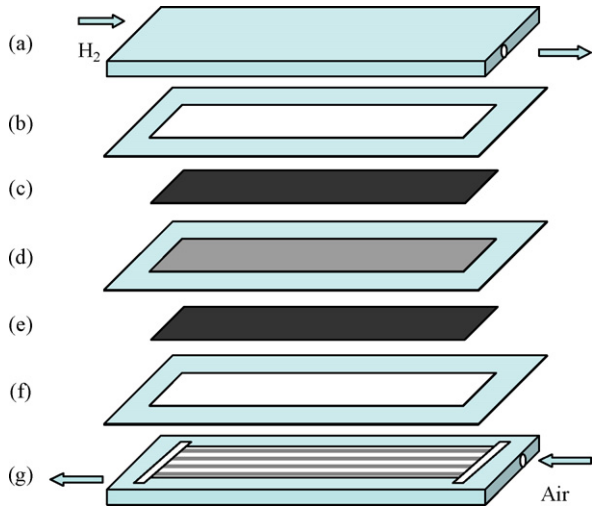

Fig. 1. Detailed view of a single cell prepared for the fuel cell operation test. (a) Carbon separator for anode, containing 16 channels, 1.0 mm wide and 0.4 mm deep between 1.0 mm wide ribs. (b) Teflon sheet used as a seal to prevent diffusion of hydrogen from the sides of the anode GDL. (c) GDL. (d) Commercially available catalyst-coated membrane (CCM) with a Pt loading of 0.3 mg cm^{-2}. (e) GDL. (f) Teflon sheet used as seal to prevent diffusion of oxygen from the sides of the cathode GDL. (g) Cathode carbon separator, containing 16 channels, 1.0 mm wide and 0.5 mm deep between 1.0 mm wide ribs. H_2 and air were supplied in a counter-flow configuration, as shown in (a) and (g).

The GDL was treated to repel water, which was prepared by submerging the GDL in a dispersion of 12 wt.% PTFE, followed by drying and heat-treatment for 15 min at 350 °C.

2.1.2. Membrane electrode assembly

The membrane electrode assembly (MEA) consisted of commercially available catalyst-coated membrane (CCM) which was sandwiched with waterproof GDLs (Section 2.1.1). The Pt loading was 0.3 mg cm^{-2} in both the anode and cathode, and the total electrode surface area was 3 cm × 15 cm.

2.1.3. Structure of the single cell

Fig. 1 shows the structure of the single cells constructed for this investigation. A single cell consisted of a CCM at the center with a GDL and carbon separator on each side. 16 straight 1 mm wide channels were machined into the separator, measuring 150 mm long; and the ribs separating the channels were 1 mm wide. The depths of the channels were 0.5 mm at the cathode and 0.4 mm at the anode. The fuel and oxidant were carried away in a counter-flow configuration.

2.1.4. Long-term operation test

Fig. 2 presents a schematic layout of the instrumentation. A fuel cell test stand (Kojima Instruments Inc., Japan) was used to evaluate the performance and characteristics of the fuel cell. The operating pressure was atmospheric pressure, the cell temperature was 75 °C, and the relative humidities of the fuel and oxidant at their respective inlets to the cell were 52 and 81% for low and high humidification, respectively. A constant current density of 0.3 A cm^{-2} was employed during the long-term test with an electric load (PLZ664WA, Kikusui Electronics Corp., Japan). A 1 kHz milliohm meter (Model 3566, Tsuruga Electric Corp., Japan) was used to take continuous measurements of the cell resistance.

2.2. Fuel cell diagnoses

The polarization curve of the cell was regularly observed during the durability test for long-term power generation. After observa-

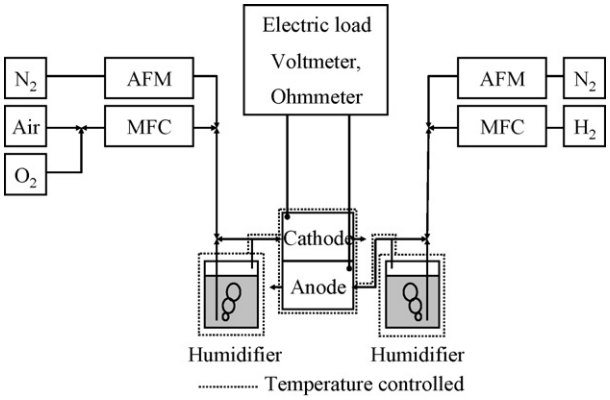

Fig. 2. Schematic diagram of the fuel cell test stand. AFC: variable area flow controller. MFC: mass flow controller. Constant gas utilization operation is available when using the MFC in synchronization with an electric load.

tions were completed, operation was stopped and the cathode gas supply was changed from air to N_2, and the electrochemical properties of the cell were then inspected. After these measurements were completed, the long-term test was re-started. Cell diagnosis was periodically conducted using such a sequence.

2.2.1. Polarization curves by galvanostatical sweep

After the long-term operation test, the polarization curves of the cell were measured under the same generating conditions, except that the load current was increased at a rate of 5 A min^{-1} to a density of 1.56 A cm^{-2} with constant gas utilization.

In the polarization curve, the cell voltage was decreased by the following factors from open-circuit voltage (OCV) E_{OCV} (see Eq. (1)): the resistance overpotential $\eta_{Resistance}$, the activation overpotential $\eta_{Activation}$, and the diffusion overpotential $\eta_{Diffusion}$. As shown in Eq. (2), $\eta_{Resistance}$ was calculated using resistance R which was measured with a 1 kHz ohm meter at the same time as the polarization measurements. In the low current density range around 0.01–0.1 A cm^{-2}, where $\eta_{Diffusion}$ can be neglected due to the low mass transport on the electrode, the logarithm of current density has a linear relationship with $\eta_{Activation}$, which is the difference between E_{OCV} and IR-free cell voltage that is the compensated $\eta_{Resistance}$. This is referred to as the Tafel equation, as shown by Eq. (3). The Tafel slope b was calculated using Eq. (3), by determining the upper limit of current density that resulted in a linear relation between $\eta_{Activation}$ and the logarithm of current density. Certain value of current density was substituted to calculate $\eta_{Activation}$. $\eta_{Diffusion}$ was estimated by subtracting the cell voltage at certain value of current density, using $\eta_{Resistance}$, and $\eta_{Activation}$ from E_{OCV} by Eq. (4). Analysis of the polarization curves in this study was based on two assumptions; negligible anode overpotential and H_2 crossover.

$$E(i) = E_{OCV} - \eta_{Resistance} - \eta_{Activation} - \eta_{Diffusion} \quad (1)$$

$$\eta_{Resistance}(i) = Ri \quad (2)$$

$$\eta_{Activation}(i) = E_{OCV} - (E(i) + \eta_{Resistance}) = b\log(i) \ (0.01 \le i \le 0.1) \quad (3)$$

$$\eta_{Diffusion}(i) = E_{OCV} - \eta_{Activation}(i) - (E(i) + \eta_{Resistance}) \quad (4)$$

2.2.2. Chronocoulometry

Chronocoulometry (CC) was used to assess degradation of the PEM [33] using a potentiostat. The model of the electrochemical system of CC to measure the H_2 gas crossover rate is shown in Fig. 3. Gas crossover rate through a PEM increases with membrane degradation. The H_2 gas crossover rate was estimated as follows: H_2 was supplied to the anode and N_2 was supplied to the cathode. The H_2 permeation from the anode through the PEM to the cathode was protonated under a 0.2 V on the cathode. Proton conducted through the PEM from the cathode to the anode. The current density was quantified as the proton conduction. The cell temperature and humidifier temperature were the same as those used during the long-term operation test. The H_2 supply rate to the anode was 0.09 L min^{-1} and the N_2 supply rate to the cathode was 0.38 L min^{-1}.

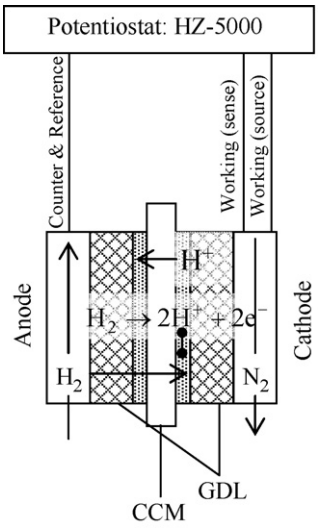

Fig. 3. The model of the electrochemical system of CC to measure the H_2 gas crossover rate.

2.3. Identification of deteriorated components

The CCM and GDL were replaced after completion of the 10 000 h operation test, as indicated in Fig. 4, and inspected to determine which component contributed more to the deterioration of the fuel cell. The spent components were replaced with a CCM and GDL that had been aged for 36 h, and the rebuilt fuel cell was operated for further diagnosis. Table 1 provides details of the combinations of these MEA components.

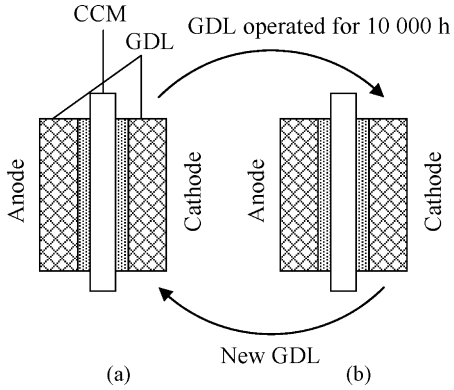

Fig. 4. Schematic diagram of the procedure used to identify components responsible for fuel cell deterioration. After completion of long-term operation tests, the cells were disassembled and the MEA (a) was removed and disassembled into its GDL and CCM components. An MEA (b), subjected to 36 h conditioning under the same operating conditions as those used for the long-term operation test, was also disassembled. Each component was then exchanged for all combinations and then re-installed for repetition of the operation test.

Table 1
Combinations of MEA components for testing to determine deteriorated components.

MEA no.	CCM	GDL
1	New	New
2	New	Operated for 10 000 h
3	Operated for 10 000 h	New
4	Operated for 10 000 h	Operated for 10 000 h

2.4. Post-analysis

After the long-term operation test was completed, the fuel cell was dismantled and the MEA was removed and also dismantled into the GDL and CCM for post-analysis. The same procedure was followed for comparison with the new (36 h aged) GDL and CCM.

2.4.1. CCM morphology and elemental analysis of the cross-section with electron probe microanalysis

An elemental mapping of the cross section of each CCM was obtained using an electron probe microanalyzer (EPMA, EPMA-1610, Shimadzu Corp., Japan) in order to evaluate deterioration of each CCM. The thickness of the PEM and the CL were also estimated from the backscattered electron images (BEIs) of the cross-section of each CCM.

2.4.2. Evaluation of the catalyst carbon support crystallinity by laser Raman spectroscopy

Laser Raman spectroscopy was employed to estimate the structural changes of the carbon support. Raman spectroscopy has been applied for many carbonaceous materials, from graphite to carbon black and activated carbon, and the spectral changes are well known to depend on the average size of the crystalline domains [35–38]. The 514.5 nm laser line was used for the excitation with approximately 1 mW of power and a 100 μm laser spot at the sample.

2.4.3. Evaluation of carbon support crystallinity by electron energy loss spectroscopy

The crystallinity of the carbon support was also evaluated by electron energy loss spectroscopy (EELS) [42,43]. Raman spectroscopy was used to observe macroscopic deterioration of the carbon support in the CL. EELS enables the observation of single particles of the carbon support and inspection of the CL on the nanometer scale. The energy loss near edge structure was examined from the surface to the interior of the carbon support particles.

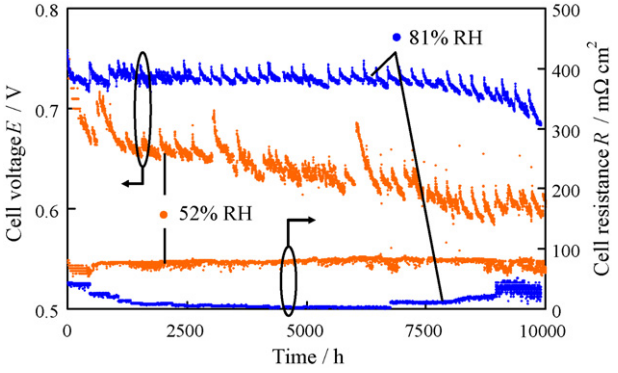

Fig. 5. Time-based voltage change during long-term operation with a current density of 0.3 A cm^{-2} under low and high humidification.

2.4.4. Measurement of pore diameter distribution in the CL using mercury intrusion porosimetry

In order to evaluate changes in the porous structure of the CL on a CCM, the distribution of pore diameters in the CL was measured using mercury intrusion porosimetry (MIP). In order to avoid destruction of the pores and the void structure, when stripping the CL from the membrane, the measurements were carried out with the CLs still on both the anode and the cathode, because small pores from the PEM applied to the CL were not detected by MIP. Therefore, the obtained pore diameter distribution was the sum of the distributions on the anode and cathode. Also, the mean thickness of the CL was measured using the BEI. This pore parameters obtained by MIP were normalized to the volumetric by dividing thickness.

3. Results

3.1. Long-term operation

3.1.1. Time-dependent cell voltage and resistance characteristics

Fig. 5 shows the changes in cell voltage and resistance with time during long-term operation with a 0.3 A cm^{-2} load. These results indicated repeated cycles of voltage decline and recovery under both high and low humidification; however, the voltage failed to return to the original level over time, indicating the long-term progression of irreversible deterioration.

The cause of these deteriorations in cell voltage during load is at 0.3 A cm^{-2}. It is difficult to observe this in detail because of relatively small mass transport; therefore, polarization curve decoupling observations were conducted at 0.8 A cm^{-2}.

Cell overpotentials during these operations were isolated from the polarization curve observed in the course of regular measure-

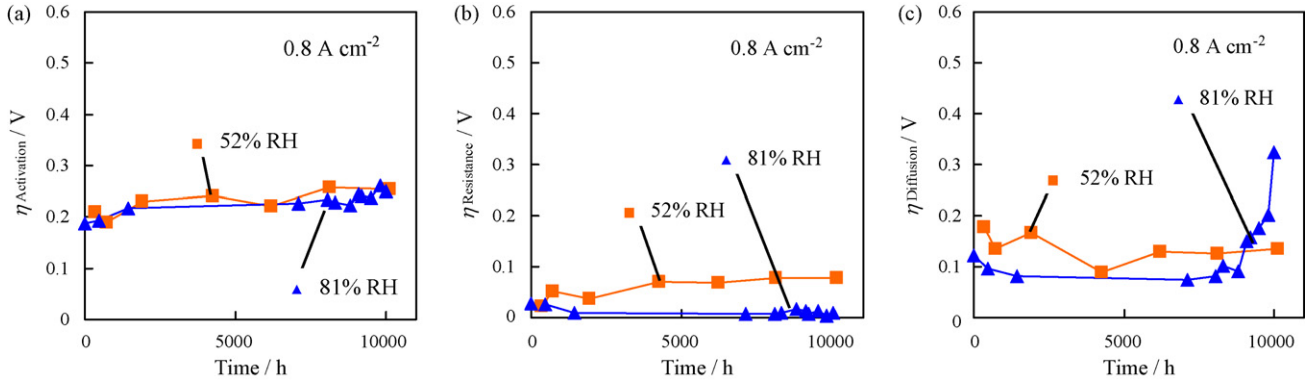

Fig. 6. (a) Activation overpotential $\eta_{Activation}$, (b) resistance overpotential $\eta_{Resistance}$, and (c) diffusion overpotential $\eta_{Diffusion}$ estimated from regular measurements of the polarization curve conducted during the long-term operation test at a current density of 0.8 A cm^{-2} under low and high humidification.

ment in order to evaluate the dominant overpotentials. Changes in gas diffusivity were especially marked under high current density; therefore, the overpotentials were isolated at a current density of 0.8 A cm^{-2}.

Fig. 6 presents the time-based changes in $\eta_{Activation}$, $\eta_{Resistance}$ and $\eta_{Diffusion}$. Under high humidification, $\eta_{Activation}$ suddenly increased up to 1400 h of operation, and then gradually increased thereafter. $\eta_{Resistance}$ displayed almost no change throughout the operation test. $\eta_{Diffusion}$ improved during the initial period and then showed only a slight increase over a long period, which indicated reasonable stability; however, after 8000 h, $\eta_{Diffusion}$ displayed an abrupt and significant increase. Under high humidification, $\eta_{Diffusion}$ was more significantly increased than $\eta_{Activation}$ or $\eta_{Resistance}$, which suggests that a key cause in cell deterioration is a decrease of gas diffusivity at CL and/or GDL.

Under low humidification, $\eta_{Activation}$ and $\eta_{Resistance}$ gradually increased throughout the operation test. $\eta_{Diffusion}$ improved during the beginning of operation and then displayed almost no change until 10 000 h. Under low humidification, $\eta_{Activation}$ tended to increase, similar to that under high humidification. Despite the almost no change under high humidification, $\eta_{Resistance}$ increased under low humidification. Conversely, $\eta_{Diffusion}$ showed almost no change under low humidification, although it had increased significantly under high humidification. These results suggest that one of the main causes of degradation in a cell under low humidification is degradation in the activity of the catalyst and degradation of the PEM.

3.1.2. Assessment of CCM degradation

The changes of the cell overpotential were considered with the results of CC. Fig. 7 shows the time-based changes in leak current density due to H_2 crossover calculated from the result of CC. The leak current density exhibited almost no change until 10 000 h under high humidification. However, under low humidification, the leak current density slowly increased after approximately 6000 h of operation. The H_2 crossover rate increases with thinning and deterioration of the membrane, and such deterioration was negligible under high humidification, but significant under low humidification. As shown in Fig. 6, there was an increase in the $\eta_{Resistance}$ of the membrane under low humidification, which may have been due to lowering of the proton conductivity that was also caused by membrane deterioration.

3.1.3. Identification of deteriorated components

In light of the changes in polarization characteristics, leak current density during the long-term operation test, it has been shown that reduced gas diffusivity at the cathode is at least one of the causes of deterioration in fuel cells under high humidification. The components of the MEA that determine gas diffusivity are the CL, which consists of a porous carbon aggregate, and the GDL, which consists of carbon fibers. In order to identify which component dominates the degradation of gas diffusivity, the components were combined as shown in Table 1 (CCM and GDL that had been operated for long-term tests and new components that had been aged for 36 h) to create rebuilt MEAs, and their polarization curves were measured. The parameters used for the 36 h aging were the same as those used in the long-term operation test.

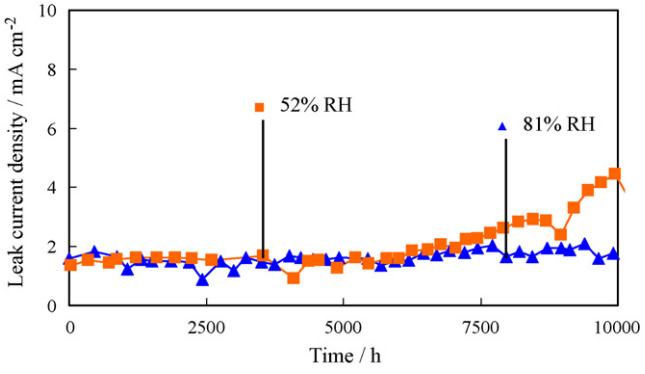

Fig. 7. Time-based changes in crossover H_2 flow rate, evaluated in terms of leak current density by CC under low and high humidification. H_2 flow rate for anode = 0.09 L min^{-1}, N_2 flow rate for cathode = 0.38 L min^{-1}. The cell voltage was set to 0.2 V.

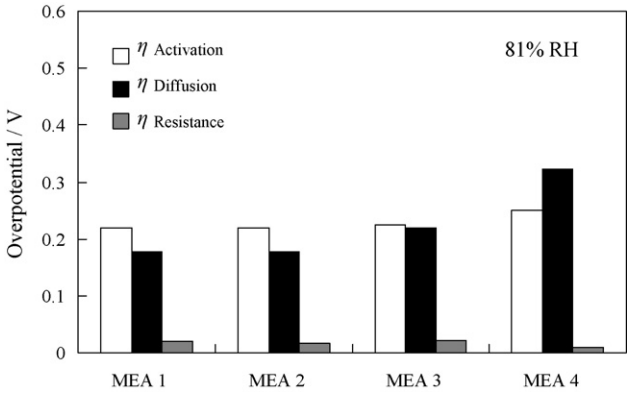

Fig. 8. Polarization separations of MEAs after exchange of components at a current density of 0.8 A cm^{-2}, as indicated in Table 1, for identification of components causing fuel cell degradation. See Fig. 3 for an explanation of the test.

Fig. 8 shows the results of the polarization separation. For MEA2, in which the GDL that had been operated for 10 000 h was paired with a new CCM, $\eta_{Diffusion}$ was same for MEA1 with a new GDL and a new CCM. In contrast, MEA3, a combination of a new GDL with a CCM that had been operated for 10 000 h has shown high $\eta_{Diffusion}$. Therefore, a new CCM should be employed to obtain high gas diffusivity, regardless of the age of the GDL.

Comparison of MEA1 and MEA2 showed that the assembly containing the GDL with 10 000 h of operation had same overpotential. However, comparison of MEA3 and MEA4 gave the result; MEA3, which contained the new GDL, exhibited lower $\eta_{Diffusion}$ than MEA4, which contained a GDL with 10 000 h of operation.

The MEAs were disassembled and their components were exchanged in an air atmosphere for the MEA2 and MEA3 tests, and measurements were then performed. The MEAs were exposed to dry air during the disassembly, and this probably caused drying of the MEA components, which accounts for the recovery in the gas diffusivity of the MEA interior.

3.2. Post-analysis

During the 10 000 h operation tests under high humidification, the gas diffusivity of the MEA at the cathode and deterioration in the CL were the main causes of degradation in fuel cell performance. Under low humidification, there was almost no cell deterioration due to reduction in the gas diffusivity but there was evidence of membrane deterioration. Post-analyses were conducted in order to clarify reasons for the deterioration of components.

3.2.1. EPMA of CCM cross-section

Fig. 9 shows the distribution of Pt on the CCM cross-sections obtained by EPMA mapping. The layer with a high concentration of Pt was the CL, and the membrane was between two CLs.

Comparison of the new components with the components employed in tests under high humidification showed that the latter

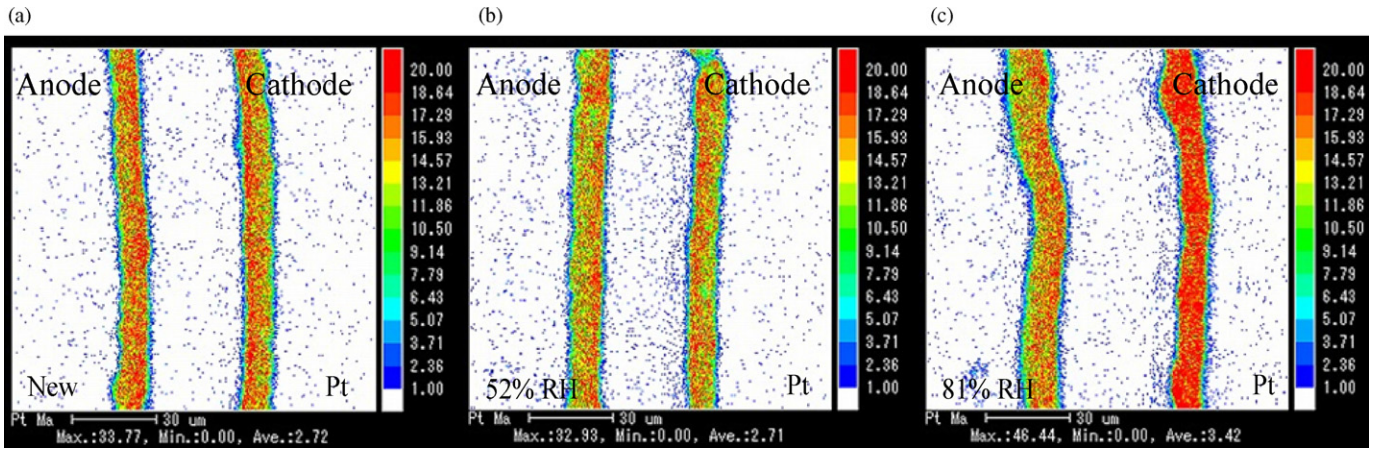

Fig. 9. Pt mapping of the CCM cross-section with EPMA. (a) New CCM. (b) CCM after 10 000 h operation at low humidification. (c) CCM after 10 000 h operation at high humidification.

had a greater increase of Pt signal in the CL, and this was particularly significant in the cathode. By contrast, the fuel cells operated under low humidification exhibited almost no change.

The thicknesses of the CL measured from the BEIs were 10.8 μm for the new anode and new cathode, 11.6 μm and 10.8 μm for the anode and cathode exposed to high humidification, and 11.4 μm and 10.3 μm for the anode and cathode exposed to low humidification, respectively.

3.2.2. Raman spectroscopy of carbon support

Fig. 10 shows Raman spectra of the carbon support of the CL. The spectral features of both the new and operated carbon support closely resembled each other. The broad G band and strong D band indicated that the carbon support had low crystallinity. For a detailed comparison of the Raman spectra, the G band position, full-width at half maximum (FWHM, denoted as ΔG) and relative band intensity (I_D/I_G) were calculated. Comparison of these parameters indicated that the operated CLs exhibited higher G band positions and smaller ΔG. This change suggested oxidation of the carbon support. Furthermore, the tendency was greater for the CLs exposed to low humidification.

In addition, for the elements exposed to low humidification, a new peak was observed in the vicinity of 1750 cm^{-1}, assigned to C=O vibration, which also suggested oxidation of the carbon support.

3.2.3. EELS of carbon supports

The previous section provided macroscopic observation of the structure of the carbon supports using Raman spectroscopy. EELS analysis of carbon particles of the new carbon support and carbon support operated under high humidification were performed. The spectra are shown in Fig. 11(c-1) and (c-2). Both superficial and

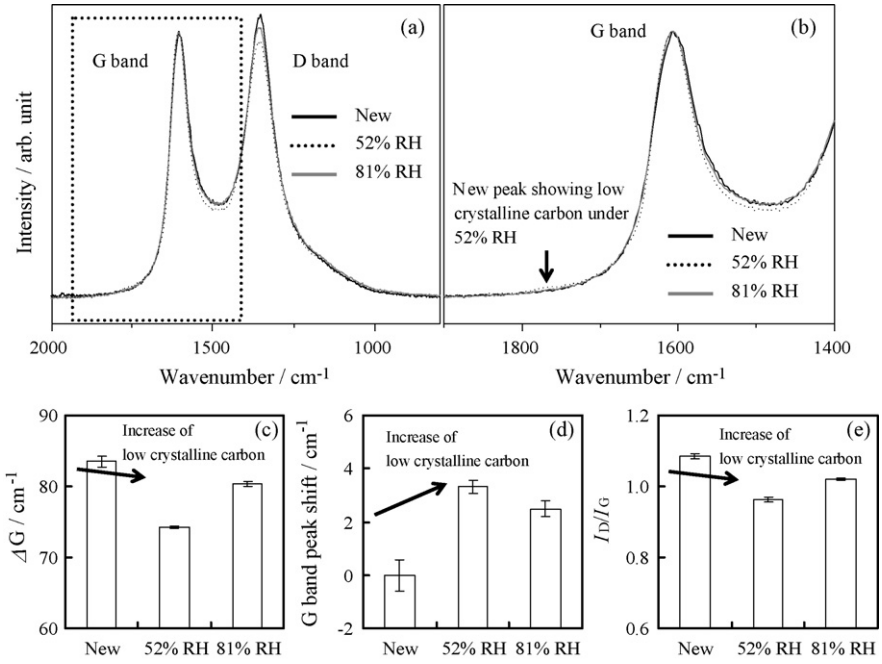

Fig. 10. Laser Raman spectra for the cathode carbon support in the vicinity of the G and D bands. Solid black lines in (a) and (b) represent results from new components. Dotted and solid gray lines represent the carbon support operated for 10 000 h under low and high humidification, respectively. (b) Expanded portion of (a) showing the G band. Left shoulder of G band under low humidification showing a new peak that was assigned to C=O vibration. (c–e) G band half-widths and shifts, and I_D/I_G, respectively, calculated from the Raman spectra.

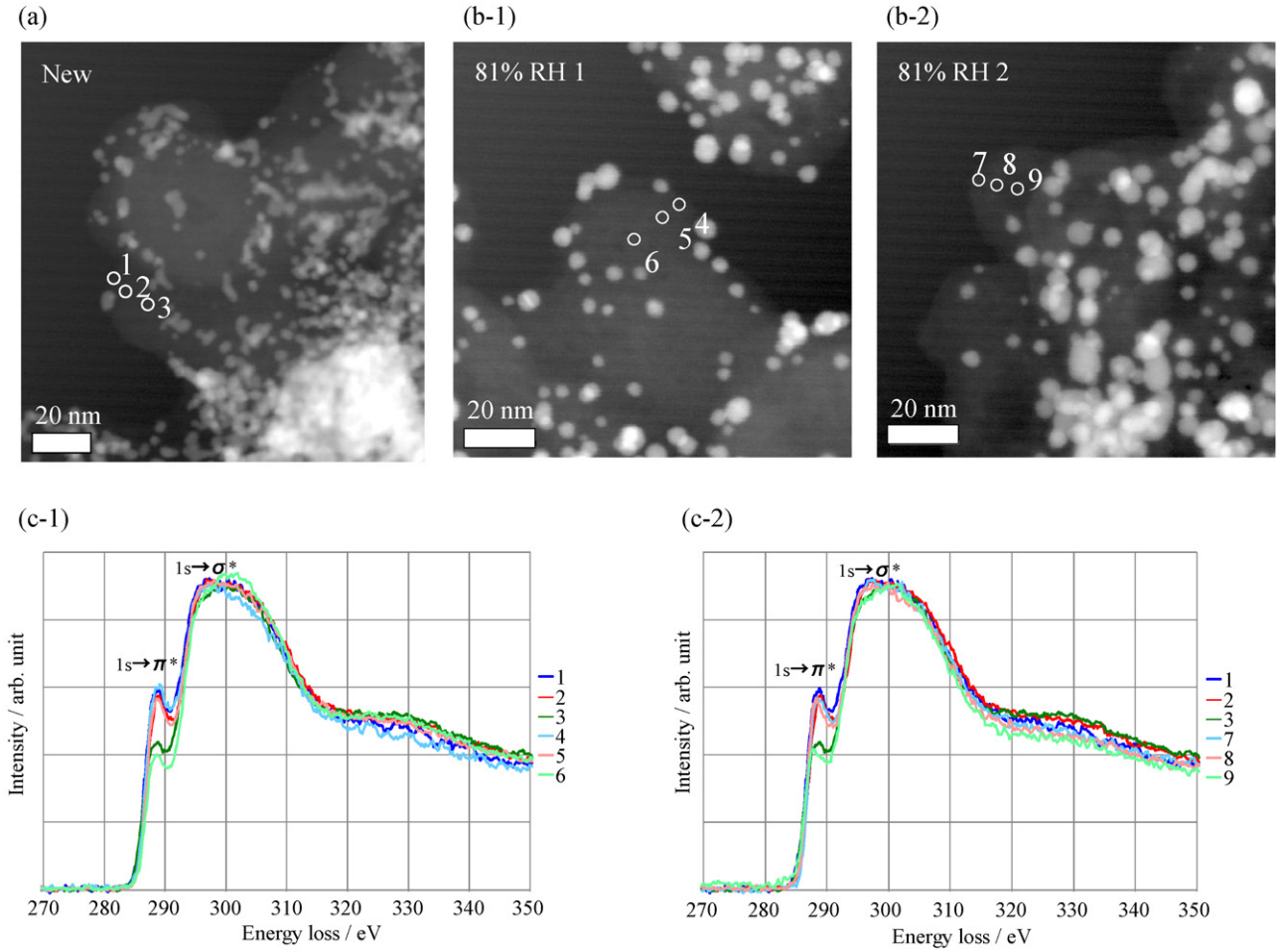

Fig. 11. Comparison of EELS spectra. EELS analysis was carried out from the surface of the carbon support into the interior, in order to evaluate the local crystallinity. The numerals on the STEM image indicate the locations where the analyses were conducted. The STEM images show (a) a new carbon support, and (b-1 and b-2) a carbon support used in the 10 000 h operation test under high humidification. (c-1) shows a comparison of the EELS spectra from 1, 2, and 3 in (a) and 4, 5, and 6 in (b-1). (c-2) shows a comparison of the EELS spectra from 1, 2, and 3 in (a) and 7, 8, and 9 in (b-2).

internal changes in the carbon particles were examined. Measurements were taken at the points from the surface into the interior shown in the STEM (Scanning Transmission Electron Microscope) images of Fig. 11(a), (b-1), and (b-2).

No significant differences were found between the new carbon particle and the carbon particles operated under high humidification. Both groups showed a large number of transitions from 1s to π^*, with more at the particle surfaces than in the interior, which indicates high fractions of hexagonal layer structures at the particle surfaces.

3.2.4. *Pore diameter distribution in the CL by MIP*

Fig. 12(a) shows the CL pore diameter distributions determined by MIP. Fig. 12(b) shows the pore volume calculated from these. The pore diameter distribution of the CL operated under high humidification was shifted to a smaller mean size than the new CL, resulting in a considerable decrease of pore volume. The mean pore diameter in the CL used under low humidification was approximately the same as that in the new CL, but the pore volume had also decreased, although the decrease was lower than that for the CL operated under high humidification. Table 2 gives a summary of the pore parameters obtained.

4. Discussion

In Fig. 6, $\eta_{\text{Diffusion}}$ increased under high humidification only during the latter period of operation, which indicates that the main cause for degradation of fuel cells was reduced gas diffusivity to the reaction sites. In addition, it is shown in Fig. 8 that the deterioration of diffusivity occurred in the CL, and that there was almost no change of diffusivity in the GDL.

Here, the results of post-analyses are discussed to clarify the cause of the degradation which mentioned above. CL corrosion can be discussed from a comparison of the Raman spectra. From previous studies of mesophase pitch, heat-treated carbon black, and models of small graphitic domains, the following estimation is possible [36–41]. Firstly, carbon with extremely low crystallinity, such as mesophase pitch, has a smaller ΔG value. The decrease of the ΔG value is derived from the decrease in the size distribution of graphitic domains contained in the sample. Secondly, carbon with small size graphitic domains exhibits relatively higher G band positions around 1600 cm^{-1} than single crystal graphite (1575 cm^{-1}). Furthermore, about the relative Raman band intensity I_D/I_G, there have been many studies on single crystal graphite and the correlation between relative Raman band intensity I_D/I_G and the crystallite length along the a axis L_a, has been determined by X-ray diffraction [35]. On the other hand, the relation between the Raman spectral shape and the crystallinity of amorphous carbon is still controversial [36–38].

Here, in Fig. 10, the carbon support after long-term operation exhibited smaller ΔG and higher G band position than the sample before long-term operation. The smaller ΔG indicates a decreased graphitic domain size distribution and the higher G band shift

Table 2
CL pore characteristics measured by MIP. V_p: pore volume. S_p: specific surface area calculated by V_p and D assuming a cylindrical pore shape. D_p: pore diameter of the peak. D_{av}: mean pore diameter calculated by $4000\,V_p/S_p$.

	Pore volume V_p cm^3 cm^{-3}	Specific surface area S_p m^2 cm^{-3}	Peak diameter D_p mm	Mean diameter D_{av} nm
New	0.44	30.6	57	58
52% RH 10 000 h	0.29	19.9	55	59
81% RH 10 000 h	0.15	13.5	42	46

indicates increasingly smaller size graphitic domains caused by oxidation. There were observed strongly under operation with low humidification. Furthermore, the new peak assigned to C=O vibration indicated that the carbon support became more amorphous under operation with low humidification. A decrease in relative Raman band intensity I_D/I_G was also observed after long-term operation. It indicated that carbon corrosion on our presumption. For single crystal graphite, a decrease in relative intensity indicates a larger, more ideal graphite domain size. However, this correlation could not be generally confirmed for the carbon with lower crystallinity. Further investigation for interpretation of the changes in relative intensity is currently in progress in our project.

Oxidation of carbon supports has been reported under high humidification [26–31] and low humidification, the latter of which appears to be carbon oxidation by hydroxyl radicals [28]. The oxidation of supports in this study was most significant under low humidification, as indicated in Section 3.2.2, which corresponds to the latter case, suggesting that hydroxyl radicals are also a factor in the weakening of the membrane, which is indicated in Section 3.1.2.

On the other hand, as calculated from the polarization curve, the diffusion overpotential in Fig. 6 showed almost no change after the 10 000 h test under low humidification, while it was significantly increased under high humidification. However, the humidifier temperature differed from that used in the test for polarization curve; therefore, simple comparisons regarding the relationship between changes in the diffusion overpotential and flooding caused by the increase in hydrophilicity due to corrosion of the CL could not be made.

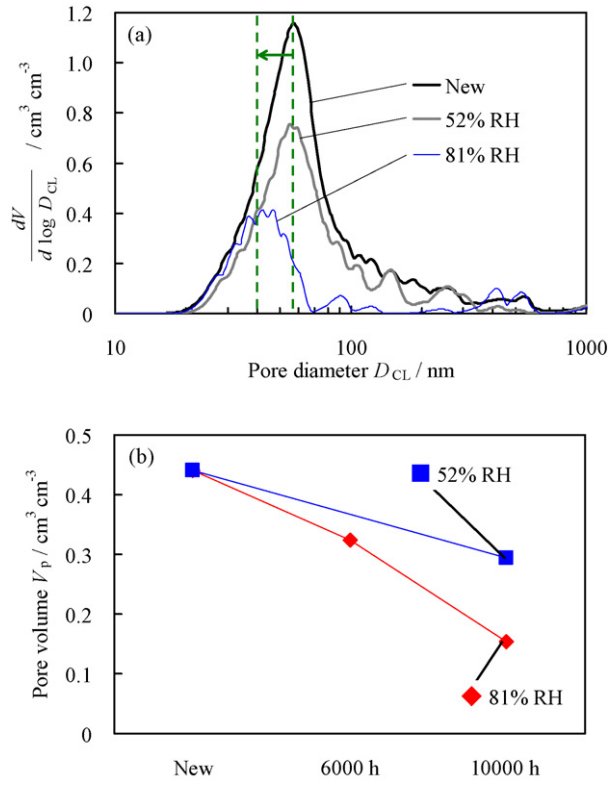

Fig. 12. (a) Comparison of porosity distributions in CLs exposed to 10 000 h operation under low and high humidification. The pore volume was estimated from the pore diameter distributions, and the time-based changes in volume are shown in (b). A greater reduction in pore volume was evident in the CL exposed to high humidification. A previously reported value [46] for pore volume after 6000 h of operation is also provided in the graph.

So the cell simulator [8] was used to project results and make observations regarding the generation of water droplets by condensation, subsequent flooding in the CL, and the relative humidity in the high current region during the polarization curve test. The simulation estimated that the relative humidity in the CL would exceed 100% under both high and low humidification, due to water generation under high current density. It appears that condensation occurred in the CL during the polarization curve test.

If the increase of $\eta_{Diffusion}$ observed during this experiment was caused by a decrease in gas diffusivity, due to clogging of the pores by water in the CL, and increased adsorption of water with increased hydrophilic character, then even under low humidification, which resulted in greater oxidation than high humidification and increased $\eta_{Diffusion}$, some increase in $\eta_{Diffusion}$ would be expected. However, there was almost no increase in $\eta_{Diffusion}$ under low humidification. The level of oxidation occurring in the previously used carbon support in this experiment suggests that flooding had not occurred.

In EELS spectra of Fig. 11, the EELS spectra show the characteristic structure of typical carbon black [45]. With respect to the disappearance of the hexagonal layer structure just under the particle surface, there were no marked differences between carbon particles that exhibited an increase in $\eta_{Diffusion}$ under the high humidification and the new particles. Oxidation of the carbon supports occurred during this experiment but it would be relatively low and it was not of sufficient intensity to cause large changes in the hexagonal layer structure of the carbon particle edges.

The pore volume and structure in the CL are also important factor to determine the diffusivity of CL.

In Fig. 12 and Table 2, the pore volume in the CL used for 10 000 h at 81% RH had much lower pore volume than that used at 52% RH, which implies that the increase in diffusion overpotential in the CL used under high humidification was due to a reduction in porosity. However, the reduction in CL thickness was quite small in comparison to the reduction in pore volume, which showed a greater tendency to decrease than expected, simply by considering the reduction in average pore diameter. The main factor influencing these changes in CL porosity was not the collapse of the CL; it seems to have been an increase in the number of isolated pores unavailable for intrusion by mercury and of extremely small pores, which acted as “bottlenecks” and whose sizes were impossible to measure.

Considering those experimental results totally, in addition, it is explained that the intensity increased with decrease in porosity and increased of the smoothness of the sample surface in analysis of porous materials such as the CL in Fig. 9. Because of higher detection efficiency scattered X-rays could be obtained from surfaces with low porosity. The intensity of scattered X-rays in the EPMA increases also with the density of Pt in the target according

to carbon disappearance by the oxidation. However, this possibility is denied because of the level of oxidation was low.

From the post-analyses, it appears that there is a large reduction in the porosity of the CL in the cathode of fuel cells under high humidification, which decreases the gas diffusivity and thereby increases the diffusion overpotential. This decrease in the CL porosity is not as significant in fuel cells under low humidification. The increase in Pt concentration found in the EPMA observations of the CL was somewhat lower in the anode, which has a greater tendency to become drier than the cathode, and in both electrodes under low humidification. The decrease in porosity of the CL was particularly marked in layers exposed to relatively high humidity. The mechanism of this deterioration is as follows: the water content of the ionomer combined with carbon black fluctuated widely, causing expansion and contraction, and this changed the porous structure of the CL, which was composed of carbon black and ionomer. This caused to reduce the porosity of the CL, and in turn, the gas diffusivity of the CL. These results indicate that the gas diffusivity that was improved by the process described in the introduction was deteriorated by long-term operation. During the lengthy 10 000 h operation test at constant 0.3 A cm^{-2}, the IV characteristics were regularly evaluated. Current densities in the IV measurements close to the limiting current density were obtained, so that lots of water was generated in the catalyst by condensation at regular intervals, and this brought about immense fluctuations in the humidity of the cell. This constitutes a very severe operating condition, and would be expected to accelerate degradation of the CL porosity.

5. Conclusions

Long-term 10 000 h operation tests of single cells were preformed with emphasis on the deterioration in gas diffusivity, using cell humidification as the parameter; and variations in overpotential were also examined. The deteriorated components were identified using rebuilt fuel cells with four different MEAs, by combining components that had previously been employed in the 10 000 h operation tests with new components. After identification of the mainly deteriorated component, post-analysis was conducted to examine the factors influencing deterioration.

Diffusion overpotential was determined to be the dominant factor in decrease of the cell voltage during operation at 81% RH. It was found that the reduction in gas diffusivity, which caused the increase in diffusion overpotential in the combinations of GDL and CL, occurred mainly in the CL; degradation of diffusivity due to the GDL was minor. In contrast, no degradation of gas diffusivity was observed operated at 52% RH.

Post-analysis of the MEA, with emphasis on deterioration of the gas diffusivity, showed that the carbon supports had similar levels of oxidation as those operated under high and low humidification; the deterioration under low humidification was slightly larger than that under high humidification, although the CL operated under high humidification exhibited a large decrease in porosity.

Therefore, the reduction of gas diffusivity due to the CL during long-term operation was caused by reduced porosity which was associated with the change of the porous structure of the CL.

The GDL was found to cause almost no reduction in gas diffusivity, even in the components used for the 10 000 h tests under high humidification. This indicates almost no change toward hydrophilic character in the components of the GDL that had been treated to repel water. No increase in hydrophilic character due to oxidation of the carbon fibers in the GDL occurred under the operating conditions in this experiment, which implied that there was almost no reduction in water repellency due to weakening or shedding of PTFE, the agent added to waterproof the GDL.

Acknowledgements

The authors express their special thanks to all those who assisted in the writing of this report. This research was performed under a grant from the Water Management Project from New Energy and Industrial Technology Development Organization (NEDO) for strategic technical development for the practical realization of PEFC. Daido University assisted in meeting the publication costs of this article.

References

[1] R. Borup, J. Meyers, B. Pivovar, Y.S. Kim, R. Mukundan, N. Garland, D. Myers, M. Wilson, F. Garzon, D. Wood, P. Zelenay, K. More, K. Stroh, T. Zawodzinski, J. Boncella, J.E. McGrath, M. Inaba, K. Miyatake, M. Hori, K. Ota, Z. Ogumi, S. Miyata, A. Nishikata, Z. Siroma, Y. Uchimoto, K. Yasuda, K. Kimijima, N. Iwashita, Chem. Rev. 107 (2007) 3904–3951.
[2] W. Schmittinger, A. Vahidi, J. Power Sources 180 (2008) 1–14.
[3] R. O'Hayre, D.M. Barnett, F.B. Prinz, J. Electrochem. Soc. 152 (2005) A439–A444.
[4] M. Watanabe, T. Motoo, Nikkashi 8 (1988) 1308–1317.
[5] M. Uchida, Y. Aoyama, N. Eda, A. Ohta, J. Electrochem. Soc. 142 (1995) 463–468.
[6] M. Uchida, Y. Aoyama, N. Eda, A. Ohta, J. Electrochem. Soc. 142 (1995) 4143–4149.
[7] M. Uchida, Y. Fukuoka, Y. Sugawara, N. Eda, A. Ohta, J. Electrochem. Soc. 143 (1995) 2245–2252.
[8] Y. Yoshikawa, T. Matsuura, M. Kato, M. Hori, J. Power Sources 158 (2006) 143–147.
[9] J. Yu, Y. Yoshikawa, T. Matsuura, M.N. Islam, M. Hori, Electrochem. Solid-State Lett. 8 (2005) A156–A158.
[10] G. Lin, W. He, T.V. Nguyen, J. Electrochem. Soc. 151 (2004) A1999–A2006.
[11] H. Yamada, T. Hatanaka, H. Murata, Y. Morimoto, J. Electrochem. Soc. 153 (2006) A1748–A1754.
[12] J.J. Kowal, A. Turhan, K. Heller, J. Brenizer, M.M. Mench, J. Electrochem. Soc. 153 (2006) A1971–A1978.
[13] G. Lin, T.V. Nguyen, J. Electrochem. Soc. 152 (2005) A1942–A1948.
[14] H. Li, Y. Tang, Z. Wang, Z. Shi, S. Wu, D. Song, J. Zhang, K. Fatih, J. Zhang, H. Wang, Z. Liu, R. Abouatallah, A. Mazza, J. Power Sources 178 (2008) 103–117.
[15] Y. Hiramitsu, K. Hirose, K. Kobayashi, M. Hori, Trans. Mater. Res. Soc. Jpn. 33 (2008) 1113–1117.
[16] Y. Hiramitsu, K. Okada, K. Kobayashi, M. Hori, Fiber Preprints 63 (2008) 192.
[17] M.V. Williams, E. Begg, L. Bonville, H.R. Kunz, J.M. Fenton, J. Electrochem. Soc. 151 (2004) A1173–A1180.
[18] K. Jiao, B. Zhou, J. Power Sources 169 (2007) 296–314.
[19] K. Jiao, B. Zhou, J. Power Sources 175 (2008) 106–119.
[20] V.P. Schulz, J. Becker, A. Wiegmann, P.P. Mukherjee, C.Y. Wang, J. Electrochem. Soc. 154 (2007) B419–B426.
[21] G. Inoue, T. Yoshimoto, Y. Matsukuma, M. Minemoto, J. Power Sources 175 (2008) 145–158.
[22] R. Borup, R. Mukundan, J. Davey, D. Wood, T. Springer, Y.S. Kim, J. Spendelow, T. Rockward, B. Pivovar, M. Arif, D. Jacobson, D. Hussey, K. Chen, K. More, P. Wilde, T. Zawodzinski, V. Gurau, W. Johnson, S. Cleghorn, DOE Hydrogen Program 2007 Annual Merit Review Procs, 2007.
[23] D. Wood, J. Davey, P. Atanassov, R. Borup, Meet. Abstr. Electrochem. Soc. 602 (2006) 641.
[24] D. Wood, J. Davey, F. Garzon, P. Atanassov, R. Borup, Meet. Abstr. Electrochem. Soc. 502 (2006) 1010.
[25] D. Wood, J. Davey, F. Garzon, P. Atanassov, R. Borup, Proc. Fuel Cell Seminar (2005), CD-ROM.
[26] J. Wang, G. Yin, Y. Shao, S. Zhang, Z. Wang, Y. Gao, J. Power Sources 171 (2007) 331–339.
[27] S. Maass, F. Finsterwalder, G. Frank, R. Hartmann, C. Merten, J. Power Sources 176 (2008) 444–451.
[28] R. Borup, J.R. Davey, F.H. Garzon, D.L. Wood, M.A. Inbody, J. Power Sources 163 (2006) 76–81.
[29] H. Shingu, C. Kaito, M. Aoki, T. Matsuura, Y. Ogawa, M. Hori, Proceedings of the 15th FCDIC Fuel Cell Symposium, 2008, pp. 86–89.
[30] M. Nose, T. Kinumoto, H.-S. Choo, Y. Iriyama, T. Abe, Z. Ogumi, Proceedings of the 15th FCDIC Fuel Cell Symposium, 2008, pp. 243–246.
[31] R.P. Ramasamya, E.C. Kumbura, M.M. Mencha, W. Liub, D. Mooreb, M. Murthyb, Int. J. Hydrogen Energy 33 (2008) 3351–3367.
[32] Y. Hiramitsu, Y. Hayashi, K. Kobayashi, M. Hori, IEEJ Trans. PE 128 (2008) 593–598.
[33] J. Yu, T. Matsuura, Y. Yoshikawa, M.N. Islam, M. Hori, Phys. Chem. Chem. Phys. 7 (2005) 373–378.
[35] F. Tunistra, J.L. Koenig, J. Chem. Phys. 53 (1970) 1126–1130.
[36] C.L. Angel, I.C. Luis, Carbon 16 (1977) 431–432.
[37] T. Gruber, T.W. Zerda, M. Gerspacher, Carbon 32 (1994) 1377–1382.
[38] A. Sadezky, H. Muckenhuber, H. Grothe, R. Niessner, U. Poschl, Carbon 43 (2005) 1731–1742.
[39] C. Castiglioni, C. Mapelli, F. Negri, G. Zerbi, J. Chem. Phys. 114 (2001) 963–974.
[40] C. Castiglioni, C. Mapelli, F. Negri, M. Rigolio, G. Zerbi, J. Chem. Phys. 115 (2001) 3769–3778.

[41] F. Negri, C. Castiglioni, M. Tommasini, G. Zerbi, J. Phys. Chem. A 106 (2002) 3306–3317.
[42] H. Naka, H. Chizawa, A. Matsunaga, N. Aoki, K. Tanaka, Y. Ogami, T. Aoki, Proceedings of the 14th FCDIC Fuel Cell Symposium, 2007, pp. 62–65.
[43] T. Aoki, H. Chizawa, H. Naka, A. Matsunaga, N. Aoki, Y. Ogami, Proceedings of the 15th FCDIC Fuel Cell Symposium, 2008, pp. 53–55.
[45] T. Harada, T. Ito, A. Masuda, Y. Otsuka, Proceedings of the 45th Battery Symposium in Japan, 2004, pp. 116–117.
[46] Y. Hiramitsu, H. Sato, K. Kobayashi, M. Hori, H. Hosomi, Y. Aoki, Y. Sakiyama, Y. Nakagawa, Proceedings of the 15th FCDIC Fuel Cell Symposium, 2008, pp. 90–93.